Clumped isotopes reveal multiple fluid sources for diagenetic cements along the Moab Fault, Utah

Sarah C. Bergman[1], Katharine W. Huntington[1], and Juliet G. Crider[1]

[1]Department of Earth and Space Sciences, University of Washington, Johnson Hall Rm-070, Box 351310, 4000 15th Avenue NE, Seattle, WA, 98195-1310

ABSTRACT. Interactions among fluids, deformational structures, and chemical changes in sediments impact deformation of the shallow crust, influencing the preservation and extraction of the economic resources it contains. These interactions have been studied along the Moab Fault, in the Paradox Basin, Utah, where diagenetic cements, joints and cataclastic deformation bands developed during faulting are thought to control fault permeability and strength. Previous fluid inclusion micro-thermometry and stable isotope data from calcite cements collected along segments of the Moab Fault suggest cements precipitated from hot, deeply circulating meteoric fluids ascending the fault. However, these methods do not measure temperature directly below ~50ºC and cannot rule out cement growth from lower-temperature fluids. Here we measure calcite cement growth-temperature directly using clumped isotope thermometry of samples collected at varying distance from fault segments dominated by joints and by deformation bands. Cement temperatures from individual segments vary greatly; cements along one joint-dominated segment indicate temperatures ranging from 57±5 to 101±1ºC (1 SE), similar to previous estimates from fluid inclusion micro-thermometry, but nearby segments reveal temperatures between 12±2 and 78±2ºC, demanding precipitation from both basinal and surficial fluid sources. The spatial pattern of cement temperatures suggests that

deformation bands effectively compartmentalize fluid flow, restricting fluid sources to warm waters thermally equilibrated with the country rock at depth in some areas, whereas joint-dominated segments enable rapid down-fault migration of cool surface waters – an interpretation that was not possible based on conventional stable isotopic data and fluid inclusions alone. Our data indicate that the relationship between faults and fluid flow can vary greatly over short length scales, with some fracture zones being highly conductive to great depths, perhaps as great as 2 km along the Moab fault.

INTRODUCTION

Brittle fault systems can serve as either conduits or barriers to fluid flow (for example, Caine and others, 1996; Davatzes and others, 2005), impacting mass and heat transfer in the crust and influencing the potential storage and migration of hydrocarbons and geothermal fluids. For fault systems in porous sandstones, two classes of structures control both hydrological and mechanical behavior during fault evolution: cataclastic deformation bands, which form tabular zones of localized deformation and crushed grains (Aydin and Johnson, 1978), and joints, which are planar fractures that show displacement normal to their surfaces and may experience subsequent shear that leads to brecciation (Myers and Aydin, 2004; Davatzes and others, 2005). While deformation bands reduce permeability within and across fault zones (Antonellini and Aydin, 1994), joints can act as significant conduits for fluid.

The development of these structures during faulting in sandstones and their influence on fluid migration has been studied in detail along the Moab fault, a large normal fault system in the Paradox Basin, Utah (Nuccio and Condon, 1996; Foxford and others, 1996, 1998; Chan and others, 2000; Davatzes and others, 2003; 2005; Eichhubl and others, 2009). Recent work highlights the importance of both structures and diagenesis in controlling fluid migration in this

and other large fault systems (Eichhubl and others, 2000; 2004; 2009; Davatzes and others, 2005; Fossen and others, 2005; Laubach and Ward, 2006; Laubach and others, 2009). Diagenetic cements precipitated along the Moab fault through time preserve information about the origin and history of the diagenetic fluids from which they grew. Based on fluid inclusion micro-thermometry and stable isotopic analysis of calcite cements from the Moab fault, previous workers have hypothesized that joints served as conduits for the ascension of warm, basinal fluids and deeply circulating meteoric waters (Chan and others, 2000; Eichhubl and others, 2009). While systematic trends were observed in $\delta^{18}O$ and $\delta^{13}C$ of calcite, and fluid inclusions from one calcite sample indicated growth temperatures of 84 to 125ºC (Eichhubl and others, 2009), diagenetic cements showed no evidence that fluid flow was directly impacted by deformation bands.

Our goal is to study the impact of deformation style on fluid circulation and cementation at Courthouse Rock along the Moab fault. We use carbonate clumped isotope thermometry (Ghosh and others, 2006; Eiler, 2007) to independently determine both the temperature and oxygen isotopic composition of the water ($\delta^{18}O_{H2O}$) from which the cements grew, revealing the direct influence of deformation style on fluid flow and cementation along the fault. Huntington and others (2011) used clumped isotopes to study the temperature and oxygen isotopic composition of diagenetic fluids, and Swanson and others (2012) applied the method to study conditions of cataclastic deformation along the Mormon Peak detachment in the Basin and Range, Nevada. However, this technique has never been applied to study the role of fault heterogeneity in controlling fluid flow in the shallow crust. Here we use clumped isotopes to test the hypothesis that calcite cements along the Moab Fault precipitated from multiple fluids, whose migration patterns were determined by the location of cataclastic deformation bands, joints and sheared

joints. At joint-dominated fault segment 5 (fig. 1), we find high temperature cements, consistent with previous hypotheses for fluid flow. However, at fault segment 2, which is characterized by both joints and deformation bands, we find a broad range of temperatures that vary spatially with distance from the fault and correlate with the location of deformation bands, providing evidence that these structures play an important role in compartmentalization of fluids in porous rocks.

STUDY AREA

The Moab fault is a basin-scale normal fault cutting Pennsylvanian – Cretaceous sedimentary units in the Paradox Basin of the southwestern United States (fig. 1; Doelling, 1985; Foxford and others, 1996; Nuccio and Condon, 1996; Davatzes and Aydin, 2003; Davatzes and others, 2005). The Moab Fault was active between the Permian and mid-Tertiary, and the last significant fault motion has been dated at 50-60 Ma from K-Ar dates in fault zone illite, indicating faulting occurred just after maximum burial (Pevear and others, 1997). Both the structural evolution and digenetic history of the Moab fault system have been studied extensively (Foxford and others, 1996; 1998; Pevear and others, 1997; Garden and others, 2001; Davatzes and Aydin, 2003; Davatzes and others, 2003; 2005; Solum and others, 2005; 2010; Eichhubl and others, 2009), making this an ideal setting to examine the relationship between structural architecture and fault permeability with new paleotemperature determinations from clumped isotope thermometry.

We analyzed calcite fault cements at Courthouse Rock, near Moab, Utah, at the intersection of the through-going southern section of the Moab fault (fault segment 1, fig. 1) and the northern section, which comprises a series of hard-linked, northwest-trending fault segments (fault segments 2-5, fig. 1; Doelling, 1985, 2002; Davatzes and others, 2003; 2005). Throughout the study area, fault segments are characterized by both cataclastic deformation bands and local

joint sets, with joints consistently overprinting deformation bands (Davatzes and Aydin, 2003; Davatzes and others, 2005). Joints occur in areas of complex fault geometry, such as at the intersection of fault segments 1 and 2 (Davatzes and Aydin, 2003; Davatzes and others, 2005). At these intersections, joints are filled with calcite cements, which are found primarily as veins and concretions along fault segment 2 in the Moab Member of the Curtis Formation (formerly mapped as the Moab Member of the Entrada Sandstone), and along fault segment 5 in the Navajo Sandstone (Eichhubl and others, 2009). These diagenetic alteration products are absent in areas of the fault characterized by deformation bands alone, suggesting that local joints occurring at intersections between segments of the Moab Fault acted as preferred fluid conduits (Foxford and others, 1996; Davatzes and others, 2005; Eichhubl and others, 2009).

SAMPLE COLLECTION AND CHARACTERIZATION

We sampled fault-related calcite for clumped isotope thermometry and trace element geochemistry from three sites along and near fault segments at Courthouse Rock (fig. 1). The sampled calcite occurs as veins and associated 2- to 3-cm-thick halos of pore-filling calcite cement surrounding veins (Eichhubl and others, 2009). Site A samples were collected immediately adjacent to fault segment 5 in the Navajo Sandstone, and site B samples were collected along three transects running perpendicular to fault segment 2 and additional locations in the Moab Member of the Curtis Formation (fig. 1). Two additional samples were collected at a third site (Site C, N38º42.5', W109º44.6') from the Moab Member of the Curtis Formation in Mill canyon, approximately 1 km west of Site B.

Millimeter-to-centimeter length prismatic calcite crystals with abundant fluid inclusions fill cm-to-dm wide joints sampled at site A. In contrast, joints at site B are mm-to-cm wide, filled with mm-to-cm length, flat, white, fibrous calcite crystals; at site C mm-to-cm length, fibrous

calcite crystals fill mm-to-cm wide joints. Minor bitumen was found at both sites A and B. Malachite also occurs at sites B and C and is thought to be the most recent cement phase at Courthouse Rock (Eichhubl and others, 2009).

Samples were characterized in thin section with transmitted light and cold-cathode cathodoluminescence (CL) microscopy to examine the textures of fault cement calcite and to help constrain the origin of diagenetic fluids. Minerals luminesce in a variety of colors based on the abundance of trace elements in the crystal lattice (Boggs and Krinsley, 2006). Calcite luminescence is typically activated by Mn^{2+} ions and quenched by Fe^{2+} ions. Under CL calcite often appears yellow-orange to red (Boggs and Krinsley, 2006).

At Courthouse Rock, cements within ~500 m of one another display markedly different CL and crystal morphology (figs. 2 and 3. Given the large amount of material needed for precise clumped isotope thermometry (~8-12 mg) and trace-element analysis (2-5 mg), some samples contain both vein and halo material, while others contain only vein material (see table 1).

CLUMPED ISOTOPE ANALYSIS AND RESULTS

Calcite samples were removed from hand samples by drilling or plucking and powdered with an agate mortar and pestle. For four of the samples, long, prismatic calcite crystals were subdivided into two to three sections parallel to the growth direction prior to powdering to examine possible temperature changes through time (table 1). Previous work indicates no measurable effect on clumped isotope analysis due to these different sampling methods (Swanson and others, 2012).

Clumped isotope samples were pre-treated by soaking in 3% H_2O_2 for 45 minutes, followed by rinsing in deionized water and freeze-drying to remove organic material. Pre-treating internal lab standards following this and similar methods does not affect conventional

stable isotope or clumped isotope measurements (Tripati and others, 2010). All samples were analyzed at the California Institute of Technology following the methods of Passey and others (2010), described here briefly. CO_2 samples were produced from 8-12 mg of calcite reacted in a common acid bath (104% H_3PO_4) at 90ºC for 10 minutes. Product CO_2 was separated from evolved H_2O via passage through multiple cryogenic traps. The CO_2 analyte was then entrained in He carrier gas and passed through a Poropak Q column in a gas chromatograph held at -20ºC. Purified CO_2 was analyzed on a modified ThermoFinnigan MAT 253 mass spectrometer configured to measure m/z ratios for masses 44-49 and screened for mass-48 contaminants. All values were referenced to Carrara marble, TV-01 calcite, and Carmel calcite standards. Measured Δ_{47} values were normalized to stochastic Δ_{47} values using heated gases (Huntington and others, 2009). Calcite growth temperature ($T(\Delta_{47})$) was calculated using the temperature equation of Guo and others (2009), which couples a theoretical model of ^{13}C-^{18}O clumping (Schauble and others, 2006) with predicted kinetic isotope effects from phosphoric acid digestion of carbonate. The theoretical temperature-clumping relationship was used because calibration data of Ghosh and others (2006) extend only from 0-50ºC. Using the calcite Δ_{47}-temperature calibration of Ghosh and others (2006) yields temperature estimates in the 0 to 50ºC range within 2 SE of temperatures calculated with the Guo and others (2009) equation, with the exception of one sample (11SB18a). We calculated $\delta^{18}O_{H2O}$ from $T(\Delta_{47})$ and measured $\delta^{18}O_{carb}$ using the calcite-water fractionation factor of Kim and O'Neil (1997).

Measured $\delta^{13}C$, $\delta^{18}O$, and Δ_{47} are presented in table 1, along with $T(\Delta_{47})$ and $\delta^{18}O_{H2O}$ calculated from weighted means of multiple analyses of individual samples. All isotopic measurements are referenced to VPDB or VSMOW as indicated in table 1. Samples were analyzed one to three times, with average values of Δ_{47} ranging between 0.471 and 0.676‰. The

161 average error in Δ_{47} for individual analyses (eight acquisitions of seven sample-standard
162 comparisons) is ± 0.010‰ (1 SE), and the average external uncertainty for replicated samples is
163 ± 0.008‰ (1 SE). The T(Δ_{47}) values correspond to calcite growth temperatures of 12 to 101ºC
164 with temperature uncertainties of ± 1 to 11ºC (1 SE). The T(Δ_{47}) values for samples representing
165 different stages of growth in the same crystal (indicated with a, b, c in sample name; table 1) are
166 indistinguishable for most samples, yielding weighted average temperatures of 79 ± 2ºC, 16 ±
167 1ºC, and 61 ± 1ºC (1 SE) for samples 11SB05, 11SB18, and 11SB25, respectively. Temperatures
168 for samples 11SB07a and 11SB07b are within 1 SE (weighted average = 75 ± 4ºC); however
169 11SB07c is significantly cooler (57 ± 5ºC). Sample average values for $\delta^{18}O_{carb}$ range from -22.3
170 to -8.5‰, and values for $\delta^{13}C$ range from -6.3 to 1.1‰, with average precisions for externally
171 replicated samples of ± 0.1‰ and ± 0.06‰, respectively (1 SE). Calculated $\delta^{18}O_{H2O}$ values range
172 from -6.2 to -14.1‰ with average uncertainties of ± 0.6‰ (1 SE). Uncertainty in $\delta^{18}O_{H2O}$ is
173 based on propagating uncertainties in both $\delta^{18}O_{carb}$ and T(Δ_{47}).

174 ## TRACE ELEMENT ANALYSIS AND RESULTS

175 A subset of the calcite samples from sites A and B were prepared for trace element
176 analysis via inductively coupled argon plasma optical emission spectroscopy (ICP-OES) at the
177 University of Washington. Powdered calcite in 2-5 mg aliquots was reacted in 3 mL of nitric
178 acid for 10 minutes to dissolve the solid $CaCO_3$. Each $CaCO_3$ – HNO_3 solution was then diluted
179 by volume to 50 mL and analyzed on a Perkin-Elmer 3300DV. ICP-OES trace element analyses
180 were performed in an attempt to further constrain variability in the origin of the fluids from
181 which samples at and within sites A and B precipitated; the results show only minor variation in
182 Ba/Ca and Sr/Ca ratios among samples from sites A and B (table 2).

183 ## DISCUSSION

Our T(Δ_{47}) results show that cements along the Moab Fault precipitated from fluids over a wide range of temperatures that varied spatially on a meter-scale. This is in marked contrast to previous interpretations based on temperature and $\delta^{18}O_{H2O}$ estimates from limited fluid inclusion micro-thermometry estimates and stable isotopes (for example Chan and others, 2000; Eichhubl and others, 2009). Warmer than Earth-surface calcite temperatures found at sites A, B, and C can be explained by previously proposed fluid circulation models (for example Morison and Parry, 1986; Chan and others, 2000; Eichhubl and others, 2009). However, cooler temperatures (<30ºC) found at site B cannot be explained by cement precipitation from deeply circulating fluids migrating up the fault near maximum burial at ~2 km depth, where it has been proposed that deformation and cementation occurred (Garden and others, 2001). Instead, we evaluate the hypotheses that clumped isotope temperatures below 30ºC reflect calcite precipitation from either 1) fluids thermally equilibrated with the host rock when it was near the surface, or 2) fluids traveling through fractures from the surface to depth sufficiently rapidly that calcite precipitated before the fluids thermally equilibrated with the host rock. Whereas the first scenario requires long-lived fluid circulation through the fracture system during both deformation and exhumation, the second scenario implies rapid penetration of surface fluids to depth along the Moab Fault prior to exhumation.

Constraints on Fluid Flow and Cementation at Site A

Based on previous stable isotopic analyses, fluid inclusion work and basin history models (Nuccio and Condon, 1996; Chan and others, 2000; Garden and others, 2001; Eichhubl and others, 2009), we anticipated that cements associated with joint-dominated segment 5 (site A; fig. 1) precipitated from volumetrically minor basinal fluids mixing with deeply circulating meteoric waters ascending the Moab fault. These meteoric waters may have been

topographically driven into the basin due to a large hydraulic head established by mid-Cenozoic laccolithic intrusions, topographically high salt anticlines, and/or uplift of the Colorado Plateau and incision of the Colorado River (Morrison and Parry, 1986; Chan and others, 2000). Previous workers have suggested that deformation and calcite precipitation likely occurred during or closely following maximum burial of the Moab Member following mid-Cenozoic faulting (Chan and others, 2000; Garden and others, 2001; Eichhubl and others, 2009). Therefore, we expected cement temperatures and isotopic compositions in the Navajo Sandstone at site A to reflect calcite precipitation from meteoric waters at temperatures near those of the host rock at maximum burial depth (~80-100ºC; constrained by basin history models, vitrinite reflectance, and Rock-Eval pyrolysis; Nuccio and Condon, 1996; Garden and others, 2001).

Our T(Δ_{47}) data from site A cluster around 70-80ºC for vein calcite samples (11SB05a, b, c and 11SB07a, b, c) and range up to 101±1ºC (1 SE) for one sample (10SB20) containing both vein and halo calcite. Calcite in sample 10SB20 occurs as pore-filling cement characterized by growth-parallel zoning, which suggest growth over an extended period of time with changing fluid trace element composition (fig. 2A). Calcite zones in this sample are commonly bright orange, red, or dark red luminescent to non-luminescent. Where bright luminescent orange cement is present, it is commonly the earliest phase of growth at the center of calcite crystals (fig. 2A). Sample 10SB20 also contains bitumen, suggesting that it precipitated from a fluid that interacted with hydrocarbons at depth. Sample 11SB05, which showed no temperature variation for subsamples a, b, and c, also shows growth parallel zoning in calcite crystals defined by bright orange to yellow luminescence. Pervasive calcite twinning is also visible under CL (fig. 2B). Samples 11SB07a and 11SB07b show no variation in temperature, similar to11SB05a, b and c. However, 11SB07c is colder than the other aliquots of calcite taken from the same crystal,

permitting as much as ~20ºC of cooling of the fluid during crystal growth. This sample shows the same bright orange to yellow luminescence as 11SB05; however it exhibits less growth-parallel zoning and calcite twinning (fig. 2C). Additionally, 11SB07c exhibits diminution of quartz grains surrounding the vein, and the calcite crystals in the vein are themselves fractured (fig. 2C), suggesting a similar fluid source but potentially more variable calcite growth conditions than 11SB05. The variability in $T(\Delta_{47})$ and in CL textures at site A suggest that different temperature calcites precipitated from different fluid sources at different times. Nevertheless, it is clear that at joint-dominated fault segment 5, all fluid sources for calcite cements observed were above earth surface temperatures.

Sample temperatures from site A are consistent with calcite cement growth from warm fluids at depth. The range of observed fluid inclusion homogenization temperatures (T_H = 84-125ºC) values for the calcite sample from site A analyzed by Eichhubl and others (2009) overlaps with the range of clumped isotope temperatures, but the highest T_H estimate exceeds measured $T(\Delta_{47})$ values as well as modeled maximum burial temperature for the host rock. Eichhubl and others (2009) suggest that cements with temperatures greater than ~100ºC likely precipitated from minor pulses of hot basinal fluids ascending the Moab Fault. Sample 10SB20 (101ºC), with its distinctive luminescence pattern (fig. 2A), may represent precipitation from one such pulse of hot basinal fluids.

The oxygen and carbon isotopic compositions of calcite cements from site A are also consistent with the hypothesis that the cements precipitated from deeply circulating meteoric waters near thermal equilibrium with the country rock at depth. Calculated $\delta^{18}O_{H2O}$ values for waters in equilibrium with site A cements range from -12 to -6 ‰, within the range of or enriched over modern meteoric waters in the Paradox Basin (-15 to -12 ‰ VSMOW; Spangler

and others, 1996) (table 1). This enrichment in ^{18}O could be attributed to a variety of factors including climate change, evaporative enrichment at the surface, or subsurface interactions between waters and host rocks. Carbon isotopic values for site A vein calcites (-6.3 to -4.4‰) are slightly depleted in ^{13}C relative to local limestones (+1 to -4‰ VPDB; Garden and others, 2001), but significantly more enriched than methanogenic carbonates (-30 to -40‰ VPDB; Boles and others, 2004; Eichhubl and others, 2009). The intermediate carbon compositions at site A and association of bitumen with calcite veins observed by ourselves and previous workers at fault segment 5 (Eichhubl and others, 2009) indicate that calcite cements precipitated from fluids that scavenged bicarbonate from local limestones, groundwater, and residual hydrocarbons during circulation through the crust.

In summary, our clumped isotope results from site A complement previous studies of diagenesis along the Moab fault, placing direct constraints on the growth temperature of calcite cements and enabling calculation of the $\delta^{18}O$ values of waters from which the cements precipitated. The temperature constraints from clumped isotopes enable interpretations of the observed variability in calcite luminescence that would not be evident from $\delta^{18}O$ and $\delta^{13}C$ values alone. The $T(\Delta_{47})$ results also provide broader context to interpret previous fluid inclusion micro-thermometry estimates, supporting the hypothesis that calcite cementation along joint sets in the Navajo Sandstone at site A was sourced from fluids migrating up the fault and occurred near maximum burial, which independent evidence suggests occurred at ca. 60-43 Ma (Nuccio and Condon, 1996; Pevear and others, 1997; Garden and others, 2001).

Constraints on Fluid Flow and Cementation at Site B

Site B is located less than 500 m northwest of the joint-based fault segment crossing site A, but the structural architecture of the fault intersection at B is defined by both joints and

deformation bands, with intense secondary jointing (fault segments 2 and 2’ respectively; fig. 1; Davatzes and others, 2005). Although the structural styles at A and B differ, published stable isotopic data for calcite cements collected at both site A and site B near fault segment 2 suggest calcite precipitated from a dominantly meteoric water source with some basinal input, giving previous workers no reason to suspect that fluid sources, temperatures, or cementation differed significantly between the two sites (Chan and others, 2000; Garden and others, 2001; Eichhubl and others, 2009). On this basis, at site B we anticipated a dominantly meteoric water source and warm clumped isotope temperatures similar to those observed at site A.

Our new carbon and oxygen isotopic data from site B within 30 m of fault segment 2 are consistent with previously published isotopic data that suggest a dominantly meteoric source for fluids ascending the fault; however, the more densely sampled calcite $\delta^{18}O$ and $\delta^{13}C$ data we collected up to 110 m from fault segment 2 suggest systematic spatial variations in diagenetic fluid sources and calcite cementation. While both our calcite $\delta^{13}C$ data and the data of Eichhubl and others (2009) range from -3.5 to +1.3‰ between fault segments 2 and 2’ (fig. 3), our new data for cements north of fault segment 2’ are all near 3‰, suggesting a change in the carbon pool from which the cements were sourced. Previous workers did not observe a systematic trend in calcite $\delta^{18}O$ value with distance (Eichhubl and others, 2009), but our additional data reveal calcite $\delta^{18}O$ and $\delta^{13}C$ values are correlated, with $\delta^{18}O_{carb}$ varying from -19 to -9‰ between fault segments 2 and 2’ and clustering around -19‰ north of segment 2’ (fig. 4). These trends suggest spatial heterogeneity of diagenetic fluid sources and calcite cementation, but the lack of independent temperature constraints makes it difficult to determine how this heterogeneity relates to the structural architecture of the fault.

The $T(\Delta_{47})$ data reveal that the temperature of the diagenetic fluids from which calcite cements grew varied considerably over distances of tens of meters, offering additional constraints on fluid sources and the mechanisms by which deformation style controls permeability along the Moab fault (fig. 5). Clumped isotope temperatures for cement samples collected north of fault segment 2' range from 44 to 70ºC, overlapping the range of temperatures observed at site A. However, cements in the zone of abundant joints between fault segments 2 and 2' range from 12 to 73ºC. The lowest temperatures in this range are too cool to record calcite precipitation from fluids migrating up the fault to ~2 km depth – the approximate depth where deformation and calcite precipitation are hypothesized to have occurred during or closely following maximum burial of the host sandstone (Nuccio and Condon, 1996; Pevear and others, 1997; Garden and others, 2001). The observed variation in $T(\Delta_{47})$ could not have been produced solely by hot fluids ascending the fault and precipitating calcite cement near maximum burial.

While the warmest cement temperatures might be explained by a fluid-cementation regime similar to that operating at site A, a fundamentally different regime varying in time and/or space must be invoked to explain the wide range of cement $T(\Delta_{47})$ values that show some cements formed at temperatures consistent with Earth-surface conditions. We propose two end-member scenarios that could explain precipitation of these low-temperature cements at site B: the cements could have grown from either 1) fluids thermally equilibrated with the host rock when it was near the surface, or 2) fluids traveling through fractures from the surface to depth sufficiently rapidly that calcite precipitated before the fluids thermally equilibrated with the host rock. In the following paragraphs we evaluate these hypotheses and explore the role of structures in controlling spatial patterns of fluid flow and cementation along the Moab fault.

In order to explain the wide range of cement temperatures observed at site B, scenario 1 would require that the fault behaved as a long-lived conduit for fluid flow throughout exhumation of the host sandstone (Curtis Formation). Initial calcite cement would have precipitated at elevated temperatures from meteoric waters circulating through the crust via joints and faults, likely initiating after mid-Cenozoic deformation of the Moab fault, similar to the scenario at site A. However, unlike site A, fluid flow and cementation at site B would have continued throughout mid to late Cenozoic exhumation of the Curtis Formation to account for the wide range of calcite T(Δ_{47}) values and low-temperature cements indicative of Earth-surface conditions.

In this scenario, we would expect cements to have meteoric water signatures, with the higher-temperature cements possibly enriched in ^{18}O and depleted in ^{13}C from interaction with silicate rocks and residual hydrocarbons at depth. The cooler cements would have formed later in the exhumation history when the host sandstone was at near-surface temperatures, with isotopic values and CL patterns suggesting shallow fluid sources. Even though fault segment 2' is dominated by deformation bands, and is therefore a baffle to cross-fault flow, if calcite precipitation continued throughout exhumation, this structure should not have prevented low-temperature surface waters from penetrating the host sandstone when it resided near the surface. Therefore, even if high-temperature cements show systematic spatial variations related to local structures, low-temperature cements should be found filling any available joints and pore spaces in the Moab Member of the Curtis Formation, regardless of structural position with respect to baffles like fault segment 2'.

While scenario 1 would lead to a decrease in cement growth temperature through time, and no relationship between structural position and the occurrence of low-temperature cements,

scenario 2 invokes highly conductive joints to enable rapid downward migration of surficial fluids and low-temperature cement growth at depth. In scenario 2, both low- and high-temperature cements could have precipitated immediately following the development of joint systems during mid-Cenozoic deformation along the Moab fault. While the low-temperature cements would have precipitated from surface waters rapidly flowing down joints and faults at Courthouse Rock, the higher-temperature cements would have formed from deeply circulating meteoric waters migrating up the fault, downward-migrating surficial fluids that had partially or completely equilibrated thermally with the host rock, or a mixture of upward- and downward-migrating fluid sources.

In scenario 2, we would expect cements to precipitate primarily from meteoric waters from both surficial and deeply circulating sources, making it difficult to distinguish this model from scenario 1 based on CL patterns and conventional $\delta^{18}O$ and $\delta^{13}C$ data alone; however, predictions for the temperature of cement growth differ for the two scenarios. In scenario 2 we would expect the coolest cements to precipitate adjacent to fault segment 2, where joint density and permeability is greatest (Davatzes and others, 2005; Eichhubl and others, 2009), and the greatest quantity of surface water might be expected to rapidly infiltrate the fault. Cements farther from fault segment 2 might record warmer temperatures, reflecting the warming of surface fluids as they migrated away from this conduit through the warm host sandstone at depth. Although this scenario does not make clear predictions of the relative timing of cementation from downward and upward migrating fluids, it does predict that cross-fault migration of cool surficial fluids would be inhibited by deformation bands, controlling the spatial pattern of cool cements at site B.

Our isotopic and T(Δ_{47}) data for the high-temperature cements from site B could be explained by either scenario, but the spatial distribution of low-temperature cements argues strongly for rapid penetration of surface waters flowing down joint-dominated faults, suggesting structural heterogeneity is responsible for cement precipitation over a wide range of temperatures prior to exhumation of the host rock. Cement temperature varies widely (range 12 to 55ºC) within 3 m of fault segment 2, suggesting either cementation over an extended period of time, or from multiple diagenetic fluids. However, sub-sampled calcite crystals did not clearly show cooling through time (table 1), and we lack constraints on the relative timing of cement growth in other samples that might suggest the warm cements precipitated when the Curtis Formation was deeply buried, while cool cements precipitated during exhumation. Therefore our clearest evidence for the source of the low-temperature cements is the spatial pattern of cement T(Δ_{47}). Although warm (50-73ºC) cements are found at distances of 3 to 109 m from fault segment 2, cool (12-28ºC) cements are limited to the highly-jointed region between fault segments 2 and 2' (fig. 5). This pattern suggests that deformation band-dominated fault segment 2' acted as a baffle for cross-fault flow of low-temperature fluids. If cool fluids were only present following significant exhumation, when the host sandstone was near the surface (scenario 1), there would be no reason to expect that fault segment 2' would act as a significant barrier for these fluids. The lack of Earth-surface temperature cements north of fault segment 2' implies that scenario 1 was not responsible for low-temperature calcite precipitation at site B.

The variability in calcite luminescence observed at site B supports the notion that cement samples with different T(Δ_{47}) values precipitated from fluids with variable Mn and Fe content (fig. 6). Calcite cement in sample 11SB19, which precipitated at low temperature (26ºC), is non-luminescent (no Mn or Fe) to weakly luminescent brownish orange (fig. 6A). There is no

evidence of calcite twinning or growth-parallel zoning in this sample. In contrast, the higher temperature samples (between 35 and 47ºC) we examined show orange to bright orange luminescence (fig. 6B). These samples also display extensive calcite twinning and occasional growth-parallel zoning, and calcite crystals within veins are fractured (fig. 6B). The luminescence of the high-temperature cements (50 to 73ºC) at site B is more variable, showing weak to extremely bright luminescence in orange, reddish-orange and yellow (fig. 6C). High-temperature calcite cements are more commonly reddish-orange than the 35-47ºC samples; however, they are distinctly different from the red luminescent calcite in sample 10SB20 at site A. Growth-parallel zoning, calcite twinning, and occasional quartz diminution characterize the high temperature samples. Overall, calcite twinning and growth-parallel zoning, as well as bright luminescence are correlated with higher calcite precipitation temperatures. However, similarly to site A, the variation in CL patterns from these samples suggests that calcite at site B precipitated from multiple diagenetic fluids.

Due to the variation in calcite growth temperature, stable isotopic composition, and CL textures of samples at site B, we propose scenario 2 is more likely responsible for the precipitation of calcite at this location. This suggests that the wide range of calcite temperatures near fault segment 2 represents cement precipitation from two sources: (a) surface waters rapidly flowing down joint-dominated faults, and (b) deeply circulating meteoric waters thermally equilibrated with the host rock at depth. This hypothesis is motivated by the $T(\Delta_{47})$ data and is also consistent with the conventional carbon and oxygen isotopic data. Calcite $\delta^{13}C$ values at site B vary with distance from fault segment 2 and are highly correlated with $T(\Delta_{47})$ (r^2=0.66), indicating that the cooler cements reflect a carbon source more enriched in ^{13}C ($\delta^{13}C$ is about -2 to 1‰) than the warmer cements ($\delta^{13}C$ is about -4 to -3‰), which approach the carbon isotopic

compositions for calcites at site A. Calculated values of $\delta^{18}O_{H2O}$ in equilibrium with the calcites at site B range from -14.1 to -7.7‰ and are not strongly correlated with $T(\Delta_{47})$ (fig. 7), suggesting a dominantly meteoric source with potentially variable contribution from basinal waters enriched in ^{18}O for all of the samples.

In summary, our observations at site B suggest cements formed from both fluids migrating up the fault zone and fluids migrating down the fault rapidly through a highly conductive joint system. Cool, down-going surficial fluids likely equilibrated thermally with the host sandstone at depth or mixed with warm fluids during fault-normal migration. Although it is possible that the lack of Earth-surface temperature cements north of fault segment 2' could be explained by thermal equilibration or mixing, the abrupt change in both $T(\Delta_{47})$ and $\delta^{13}C$ at fault segment 2' suggests that deformation bands acted as a barrier to cross-fault flow for these down-going surficial fluids. While fluids moving down and away from the major joint-dominated fault at site B (fault segment 2) were effectively compartmentalized by this barrier, deeply circulating meteoric fluids (thermally equilibrated with the host rock) precipitated throughout site B, providing strong evidence for structural control of hydrologic behavior and cementation along the Moab fault.

Predictions and Constraints on Fluid Flow and Cementation at Site C

Varying cement geochemistry at sites A and B indicates diagenetic calcite precipitated from multiple fluid sources that were compartmentalized into different regions by local structures. These observations suggest that cement fluid source and temperature might be predicted at site C (fig. 1) based on the local structures associated with the cements in this location.

Site C is located at the intersection of fault segments 2b, 2c and 3 (as determined by Davatzes and others, 2005), and is characterized by both joints and deformation bands. Thus we might expect cements precipitated from hot, deep sources like at sites A and B far from the fault, as well as from shallow, cool sources similar to site B near fault segment 2. Although we present $T(\Delta_{47})$ data for only two cement samples from site C, our results for this site are broadly consistent with the hypothesis of precipitation from multiple fluid sources. The first sample at site C yields a $T(\Delta_{47})$ value of 78°C; this result is similar to average temperatures at site A and the highest temperatures at site B, and is consistent with estimated temperatures of the country rock during maximum burial. The second sample at this site yields a $T(\Delta_{47})$ value of 41°C, which is within the range of temperatures observed for cements collected within 30 m of fault segment 2 at site B, and significantly cooler than expected for fluids ascending the fault following deformation near maximum burial. These samples plot on the $\delta^{13}C$ vs. $T(\Delta_{47})$ trend defined by the site A and B samples (fig. 7), and are broadly consistent with the hypothesis that fluid migration and cementation near Courthouse Rock are controlled by local structures.

Based on our observations from calcite cements at sites A, B, and C, it appears that deeply circulating meteoric waters migrated throughout the entire study area, while down-going surface waters penetrated rapidly to significant depth only along joint-dominated faults and were effectively compartmentalized by deformation bands. Carbon and oxygen isotopic data, CL microscopy, and other observations of previous workers are consistent with our findings that the structural architecture influences fluid flow and cementation in this area (Eichhubl and others, 2009). However, these previous datasets alone do not show the clear influence of deformation style on fluid flow or hint that joint-dominated faults can be such effective conduits for rapid downward flow of surficial fluids. Our detailed model for the relationship among deformation

style, fluid flow and cementation along the Moab fault would not have been possible without clumped isotope thermometry.

CONCLUSIONS

In contrast to the interpretation based on conventional stable isotopic and fluid inclusion data alone, our T(Δ_{47}) data indicate the relationship between faults and fluid flow can vary greatly over short length scales, with some fracture zones being highly conductive to great depths, possibly up to 2 km along the Moab fault. While previous models of calcite precipitation from deeply circulating meteoric waters ascending the Moab Fault can account for the precipitation of above Earth-surface temperature cements, this model must be adjusted to account for Earth-surface temperature calcites found at site B. We propose that in addition to precipitating from upward migrating fluids as proposed by Chan and others (2000) and Eichhubl and others (2009), calcite cements also precipitated from cool fluids traveling through fractures from the surface to depth rapidly enough and in large enough quantities that precipitation could occur before the fluids warmed to ambient conditions at depth. Without clumped isotope thermometry, we would not recognize the significant role that cool fluids played in calcite growth at Courthouse Rock. [add more general statement about the role of structures in compartmentalizing fluids in porous rx in general… conclusions should look like a triangle, starting narrow at the top and ending broadly at the bottom.]

ACKNOWLEDGMENTS

Acknowledgment is made to the donors of the American Chemical Society Petroleum Research Fund for support of this research (ACS-PRF grant 49709 to KWH). We thank John Eiler, Nami Kitchen and Ron Sletten for generous laboratory access and assistance. We thank Gerd Winterleitner and David Birlenbach for field assistance, and Winterleitner, David Budd,

and Peter Eichhubl for discussions that guided our thinking on this project.

REFERENCES CITED

Antonellini, M. and Aydin, A., 1994, Effect of faulting on fluid flow in porous sandstones: petrophysical properties: AAPG Bulletin, v. 78.

Aydin, A., and Johnson, A.M., 1978, Development of faults as zones of deformation bands and as slip surfaces in sandstone. Pure and Applied Geophysics: v. 116, p. 931–942.

Boggs, S., and Krinsley, D., 2006, Application of cathodoluminescence imaging to the study of sedimentary rocks: Cambridge, Cambridge University Press, 165 p.

Boles, J.R., Eichhubl, P., Garven, G., and Chen, J., 2004, Evolution of a hydrocarbon migration pathway along basin-bounding faults: evidence from fault cement: AAPG Bulletin, v. 88, p. 947–970.

Caine, J.S., Evans, J.P., and Forster, C.B., 1996, Fault zone architecture and permeability structure: Geology, v. 24, p. 1025–1028.

Chan, M.A., Parry, W.T., and Bowman, J.R., 2000, Diagenetic hematite and manganese oxides and fault-related fluid flow in Jurassic sandstones, southeastern Utah: AAPG Bulletin, v. 84, p. 1281–1310.

Davatzes, N., and Aydin, A., 2003, Overprinting faulting mechanisms in high porosity sandstones of SE Utah: Journal of Structural Geology, v. 25, p. 1795–1813.

Davatzes, N.C., Aydin, A., and Eichhubl, P., 2003, Overprinting faulting mechanisms during the development of multiple fault sets in sandstone, Chimney Rock fault array, Utah, USA: Tectonophysics, v. 363, p. 1–18.

Davatzes, N.C., Eichhubl, P., and Aydin, A., 2005, Structural evolution of fault zones in sandstone by multiple deformation mechanisms: Moab fault, southeast Utah: Geological Society of America Bulletin, v. 117, p. 135–148.

Doelling, H., 1985, Geologic map of Arches National Park and vicinity, Grand County, Utah: Utah Geological and Mineral Survey, Salt Lake City, Utah, scale 1:50,000.

Doelling, H., 2002, Geologic map of the Moab 7.5’ quadrangle, Grand County, Utah: Utah Geological Survey, Utah Dept. of Natural Resources, Salt Lake City, Utah.

Eichhubl, P., Greene, H., Naehr, T., and Maher, N., 2000: Structural control of fluid flow: offshore fluid seepage in the Santa Barbara Basin, California: Journal of Geochemical Exploration, v. 69–70, 545–549.

Eichhubl, P., Taylor, W.L., Pollard, D.D., and Aydin, A., 2004: Paleo-fluid flow and deformation in the Aztec sandstone at the Valley of Fire, Nevada—evidence for the coupling of hydrogeologic, diagenetic, and tectonic processes: Geological Society of America Bulletin, v. 116, p. 1120–1136.

Eichhubl, P., Davatz, N.C., and Becker, S.P., 2009, Structural and diagenetic control of fluid migration and cementation along the Moab fault, Utah: AAPG Bulletin, v. 93, p. 653–681.

Eiler, J.M., 2007, “Clumped-isotope” geochemistry—The study of naturally-occurring, multiply-substituted isotopologues: Earth and Planetary Science Letters, v. 262, p. 309–327.

Ferrill, D.A., Morris, A.P., Evans, M.A., Burkhard, M., Groshong Jr., R.H., and Onasch, C.M., 2004, Calcite twin morphology: a low-temperature deformation geothermometer: Journal of Structural Geology, v. 26, p. 1521–1529.

Fossen, H., Johansen, T.E.S., Hesthammer, J., and Rotevatn, A., 2005, Fault interaction in porous sandstone and implications for reservoir management; examples from southern Utah: AAPG Bulletin, v. 89, p. 1593–1606.

Foxford, K.A., Garden, I.R., Guscott, S.C., Burley, S.D., Lewis, J.J.., Walsh, J.J., and Watterson, J., 1996, The field geology of the Moab fault, in: Geology and Resources of the Paradox Basin: Utah Geological Association Guidebook. p. 265–283.

Foxford, K.A., Walsh, J.J., Watterson, J., Garden, I.R., Guscott, S.C., and Burley, S.D., 1998, Structure and content of the Moab fault zone, Utah, USA, and its implications for fault seal prediction *in* Geological Society, London, Special Publications, v. 147, p. 87–103.

Garden, I.R., Guscott, S.C., Burley, S.D., Foxford, K.A., Walsh, J.J., and Marshall, J., 2001, An exhumed palaeo-hydrocarbon migration fairway in a faulted carrier system, Entrada Sandstone of SE Utah, USA: Geofluids, v. 1, p. 195–213.

Ghosh, P., Adkins, J., Affek, H., Balta, B., Guo, W., Schauble, E.A., Schrag, D., and Eiler, J.M., 2006, $^{13}C–^{18}O$ bonds in carbonate minerals: A new kind of paleothermometer: Geochimica et Cosmochimica Acta, v. 70, p. 1439–1456.

Goldstein, R., and Reynolds, J., 1994, Systematics of fluid inclusions in diagenetic minerals *in* SEPM Short Course 31, Tulsa, Oklahoma, 199 p.

Guo, W., Mosenfelder, J.L., Goddard III, W.A., and Eiler, J.M., 2009, Isotopic fractionations associated with phosphoric acid digestion of carbonate minerals: Insights from first-principles theoretical modeling and clumped isotope measurements: Geochimica et Cosmochimica Acta 73, p. 7203–7225.

Huntington, K.W., Eiler, J.M., Affek, H.P., Guo, W., Bonifacie, M., Yeung, L.Y., Thiagarajan, N., Passey, B., Tripati, A., Daëron, M., and Came, R., 2009, Methods and limitations of "clumped" CO_2 isotope (Δ_{47}) analysis by gas-source isotope ratio mass spectrometry: Journal of Mass Spectrometry, v. 44, p. 1318–1329.

Huntington, K.W., Budd, D.A., Wernicke, B.P., and Eiler, J.M., 2011, Use of clumped-isotope thermometry to constrain the crystallization temperature of diagenetic calcite: Journal of Sedimentary Research, v. 81, p. 656–669.

Hurlow, H., and Bishop, C.E., 2003, Recharge areas and geologic controls for the Courthouse-Sevenmile Spring system, Western Arches National Park, Grand County, Utah: Utah Geological Survey Special Study, Salt Lake City, Utah, v. 108, 55 p.

Kerrich, R., Latour, T., and Willmore, L., 1984, Fluid participation in deep fault zones - evidence from geological, geochemical, and O-18/O-16 relations: Journal of Geophysical Research, v. 89, p. 4331–4343.

Kim, S.-T., and O'Neil, J.R., 1997, Equilibrium and nonequilibrium oxygen isotope effects in synthetic carbonates: Geochimica et Cosmochimica Acta, v. 61, p. 3461–3475.

Laubach, S.E., and Ward, M.E., 2006, Diagenesis in porosity evolution of opening-mode fractures, Middle Triassic to Lower Jurassic La Boca Formation, NE Mexico: Tectonophysics, v. 419, p. 75–97.

Laubach, S.E., Olson, J.E., and Eichhubl, P., 2009, Fracture Diagenesis and Producibility in Tight Gas Sandstones, *in* Unconventional Energy Resources: Making the Unconventional Conventional, 29th Annual GCSSEPM Foundation Annual Bob. F. Perkins Research Conference Proceedings, (ed.) Carr, T., D'Agostino, T., Ambrose, W., Pashin, J., and Rosen, N.C., v. 29, p. 483-499.

Morrison, S.J., and Parry, W.T., 1986, Formation of carbonate-sulfate veins associated with copper ore deposits from saline basin brines, Lisbon Valley, Utah; fluid inclusion and isotopic evidence: Economic Geology, v. 81, p. 1853–1866.
Myers, R., and Aydin, A., 2004, The evolution of faults formed by shearing across joint zones in sandstone: Journal of Structural Geology, v. 26, p. 947–966.
Nuccio, V., and Condon, S., 1996, Burial and thermal history of the Paradox Basin, Utah and Colorado, and petroleum potential of the middle Pennsylvanian Paradox Formation: U.S. Geological Survey Bulletin 2000-0.
Oliver, J., 1992, The spots and stains of plate tectonics: Earth-Science Reviews, v. 32, p. 77–106.
Passey, B.H., Levin, N.E., Cerling, T.E., Brown, F.H., and Eiler, J.M., 2010, High-temperature environments of human evolution in east Africa based on bond ordering in paleosol carbonates: Proceedings of the National Academy of Sciences, v. 107, p. 11245–11249.
Pevear, D., Vrolijk, P., and Lomgstaffe, F., 1997, Timing of Moab fault displacement and fluid movement integrated with burial history using radiogenic and stable isotopes, in: Contributions to the Second International Conference on Fluid Evolution, Migration and Interaction in Sedimentary Basins and Orogenic Belts. Presented at the Geofluids II Conference, The Queen's University of Belfast, Belfast, Northern Ireland, p. 42–45.
Schauble, E.A., Ghosh, P., and Eiler, J.M., 2006, Preferential formation of ^{13}C–^{18}O bonds in carbonate minerals, estimated using first-principles lattice dynamics: Geochimica et Cosmochimica Acta, v. 70, p. 2510–2529.
Solum, J.G., Davatzes, N.C., and Lockner, D.A., 2010, Fault-related clay authigenesis along the Moab Fault: Implications for calculations of fault rock composition and mechanical and hydrologic fault zone properties: Journal of Structural Geology, v. 32, p. 1899–1911.
Solum, J.G., van der Pluijm, B.A., and Peacor, D.R., 2005, Neocrystallization, fabrics and age of clay minerals from an exposure of the Moab Fault, Utah: Journal of Structural Geology, v. 27, p. 1563–1576.
Spangler, L.E., 1996, Hydrology, chemical quality, and characterization of salinity in the Navajo aquifer in and near the Greater Aneth Oil Field, San Juan County, Utah, by Spangler, L.E., D.L. Naftz, and Z.E. Peterman; prepared in cooperation with the U.S. Environmental Protection Agency.
Swanson, E.M., Wernicke, B.P., Eiler, J.M., and Losh, S., 2012, Temperatures and fluids on faults based on carbonate clumped–isotope thermometry, American Journal of Science, v. 312, p. 1–21.
Tripati, A.K., Eagle, R.A., Thiagarajan, N., Gagnon, A.C., Bauch, H., Halloran, P.R., and Eiler, J.M., 2010, ^{13}C–^{18}O isotope signatures and "clumped isotope" thermometry in foraminifera and coccoliths: Geochimica et Cosmochimica Acta, v. 74, p. 5697–5717.

FIGURE CAPTIONS

Fig. 1. (A) Geologic map and cross section of the Moab fault system at Courthouse Rock modified following Davatzes and others (2005), Doelling and others (2006), and Eichhubl and others (2009). Fault segments referenced in the text are numbered following Davatzes and others (2005). Site C, which is not indicated on the map, is located in the Moab Member of the Curtis

608 Formation along fault segment 2, ~1 km west of Site B. (B) Moab Member of the Curtis
609 Formation at the intersection of fault segments 1 and 2 (Site B), after Eichhubl and others (2009),
610 with sample locations (see Table 1).
611 Fig. 2. Photomicrographs of calcite samples under CL. (A) CL images for samples from site A,
612 which are characterized by bright orange luminescence, calcite twinning, and growth-parallel
613 zoning in calcite crystals, as described in the text. (B) CL images for samples from site B,
614 grouped by cement growth temperature indicated by clumped isotope thermometry. These
615 samples are characterized by non-luminescent orange to extremely bright yellow-orange
616 luminescence, as well as growth-parallel zoning, calcite twinning, quartz diminution, and calcite
617 crystal fracture as described in the text.
618 Fig. 3. Distance north of fault segment 2 versus $\delta^{13}C$ for samples from site B. The
619 greatest variation in carbon composition occurs in the heavily jointed region between fault
620 segments 2 and 2' (0-30 m on the figure). Analytical uncertainty (1 SE) in $\delta^{13}C$ is smaller than
621 the symbol size.
622 Fig. 4. Distance north of fault segment 2 versus $\delta^{18}O_{carb}$ for samples from site B.
623 Analytical uncertainty (1 SE) in $\delta^{18}O_{carb}$ is indicated where the uncertainty is larger than the
624 symbol size. The greatest variation in the oxygen isotopic composition of calcite cements occurs
625 in the heavily jointed region between fault segments 2 and 2'. Based on $\delta^{18}O_{carb}$ data alone it is
626 not possible to determine if the variation reflects variation in fluid temperature, isotopic
627 composition, or both.
628 Fig. 5. Distance north of fault segment 2 versus $T(\Delta_{47})$ for samples from site B. Symbol
629 shading indicates the oxygen isotopic composition of the fluid from which the cement

precipitated ($\delta^{18}O_{H2O}$, VSMOW). Error bars represent 1 SE uncertainty in $T(\Delta_{47})$; where error bars are not visible, the uncertainty is smaller than the symbol size

Fig. 6. Calculated $\delta^{18}O_{H2O}$ versus $T(\Delta_{47})$ for all samples at sites A, B, and C. Error bars represent 1 SE uncertainty, and where not visible are smaller than symbol size. There is no correlation between fluid isotopic composition and calcite precipitation temperature, indicating diagenetic cements precipitated from fluids with a range of oxygen isotopic compositions over a wide range of temperatures as discussed in the text.

Fig. 7. $\delta^{13}C$ versus $T(\Delta_{47})$ for all samples at sites A, B, and C. Error bars represent 1 SE uncertainty, and where not visible are smaller than symbol size. Cement temperature and carbon isotopic composition are correlated at site B ($r^2 = 0.66$), indicating changes in the carbon pool with changing calcite precipitation temperature, and therefore changing diagenetic fluid source

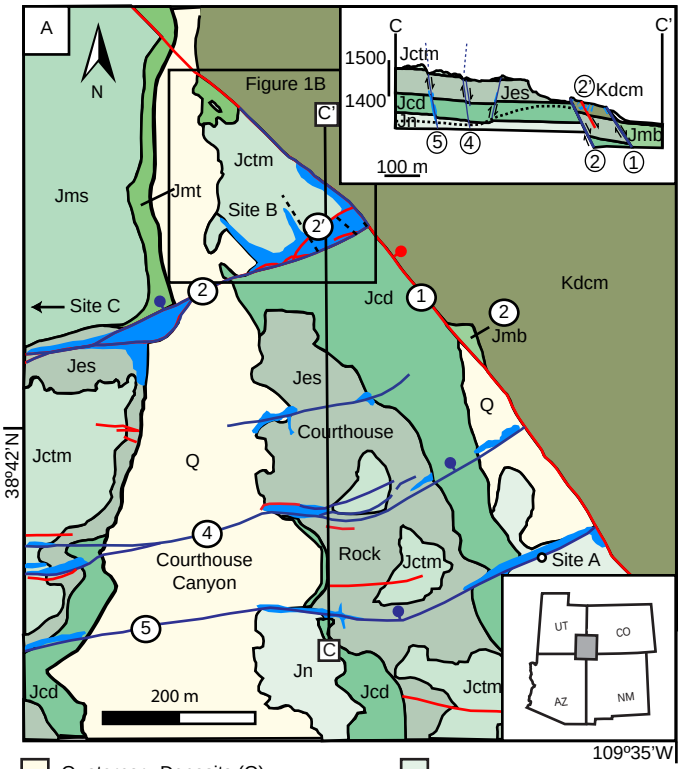

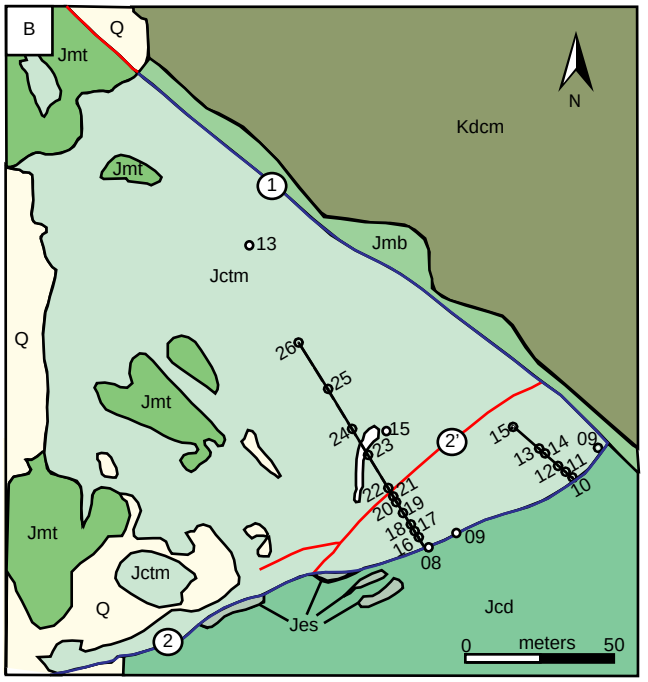

- Quaternary Deposits (Q)
- Dakota Sandstone and Cedar Mountain Formation, undivided (kdcm)
- Brushy Basin Member (Jmb)
- Salt Wash Member (Jms)
- Tidwell Member (Jmt)
- Moab Member (Jctm)
- Slick Rock Member (Jes)
- Dewey Bridge Member (Jcd)
- Navajo Sandstone (Jn)
- Carbonate cement
- Fault (ball on hanging wall)
- Joint-based fault
- Deformation band-based fault
- Sample Ttransect
- 2010 sample
- 2011 sample

Site A

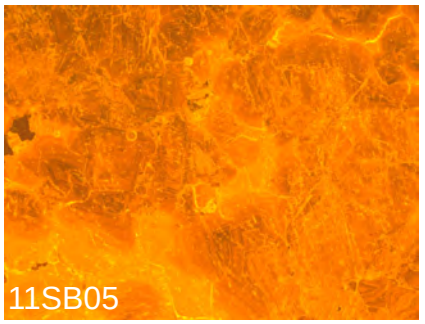

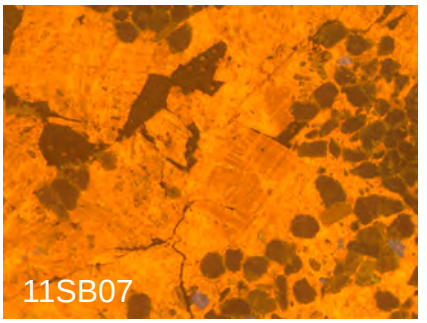

Site B

<30ºC

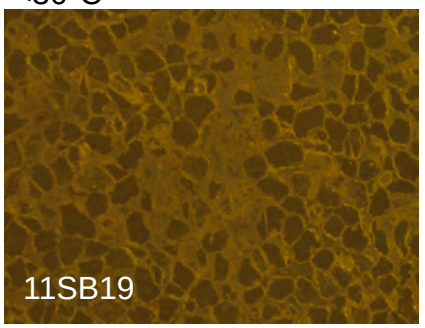

30-50ºC

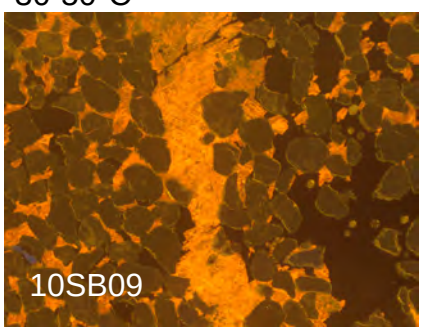

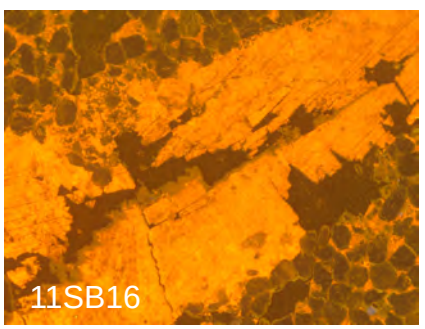

50-70ºC

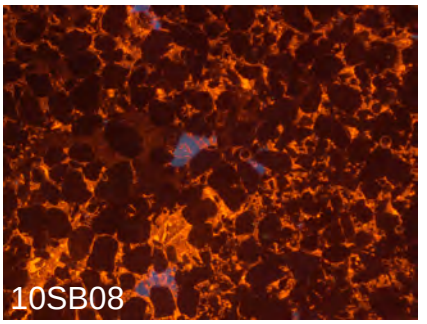

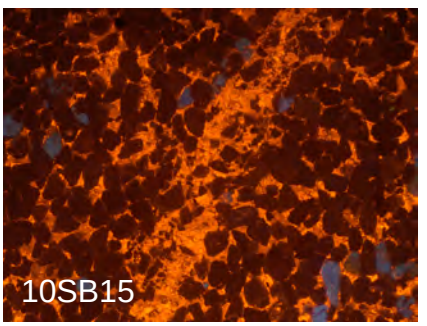



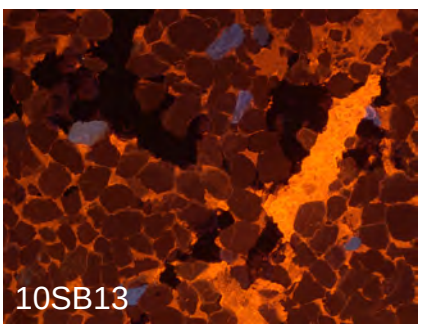

>70ºC

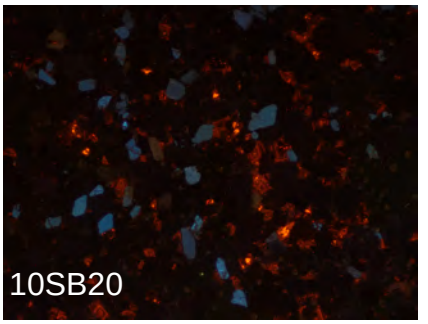

Site A

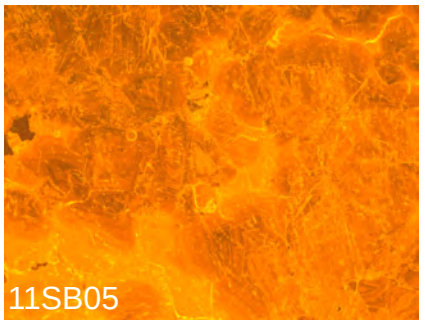

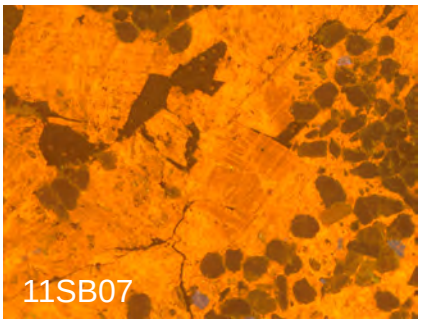

Site B

<30ºC

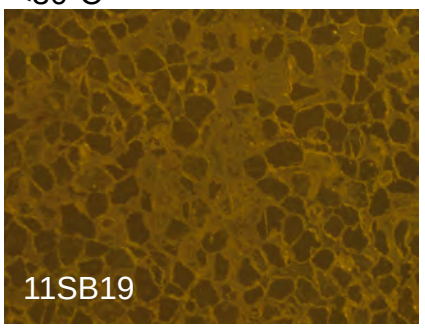

30-50ºC

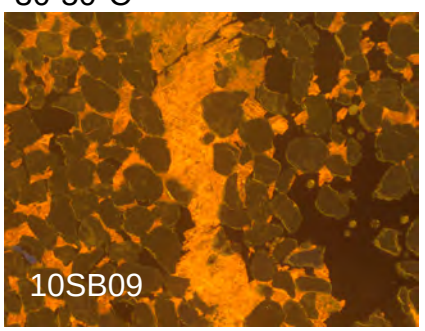

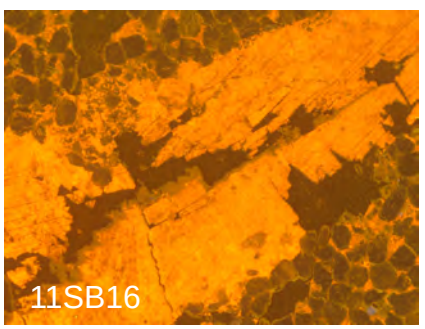

50-70ºC

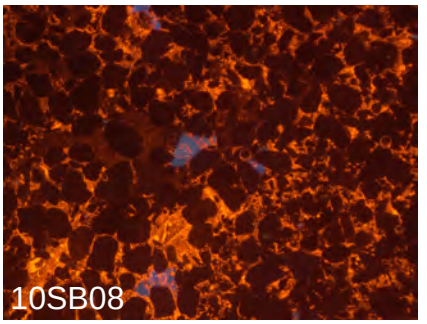

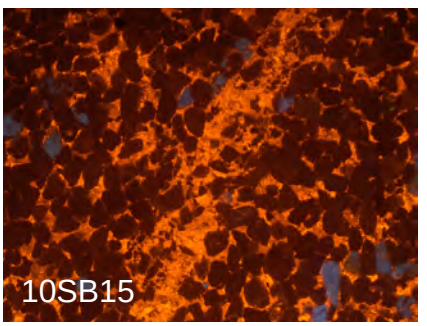



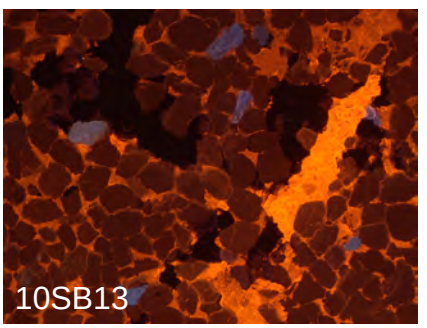

>70ºC

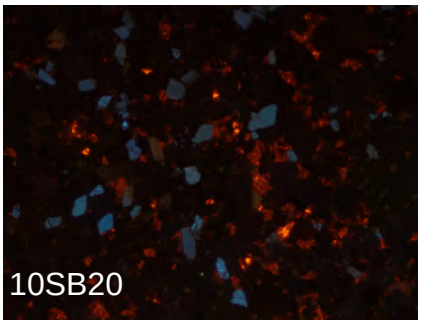

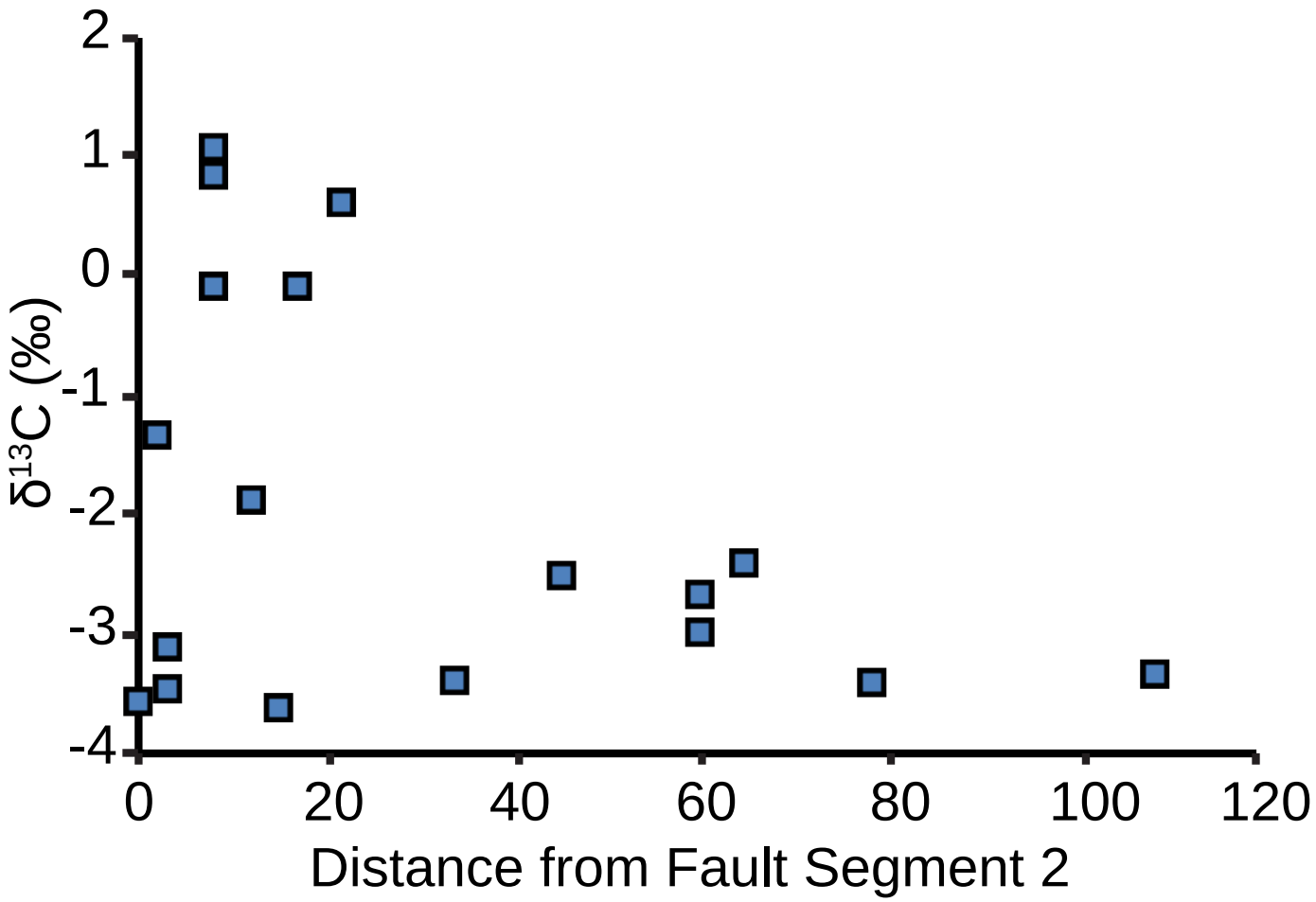
2
1
0
-1
-2
-3
-4
δ13C (‰)
0
20
40
60
80
100
120
Distance from Fault Segment 2

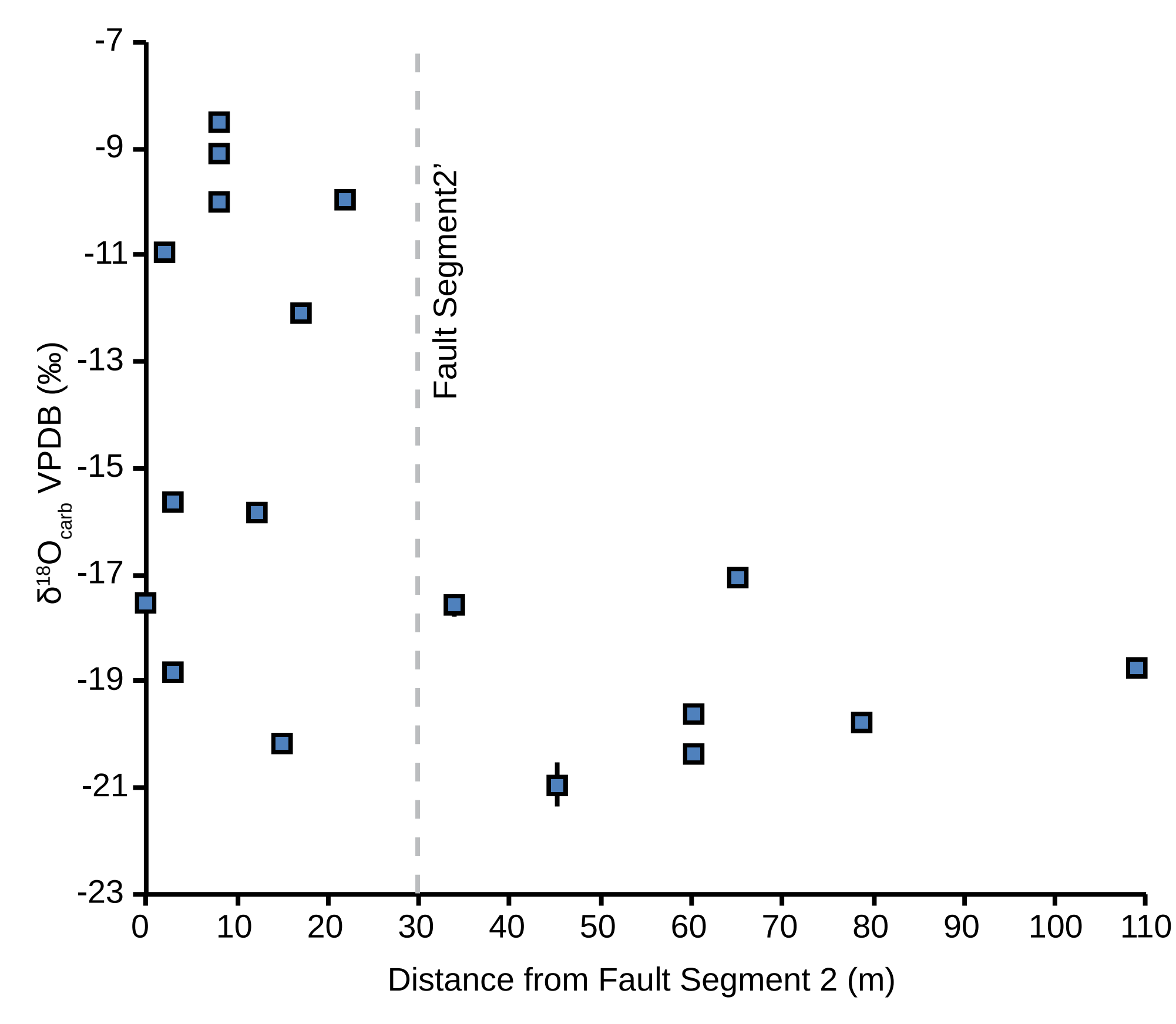
-7
-9
-11
-13
-15
-17
-19
-21
-23
δ18Ocarb VPDB (‰)
Fault Segment2'
0
10
20
30
40
50
60
70
80
90
100
110
Distance from Fault Segment 2 (m)

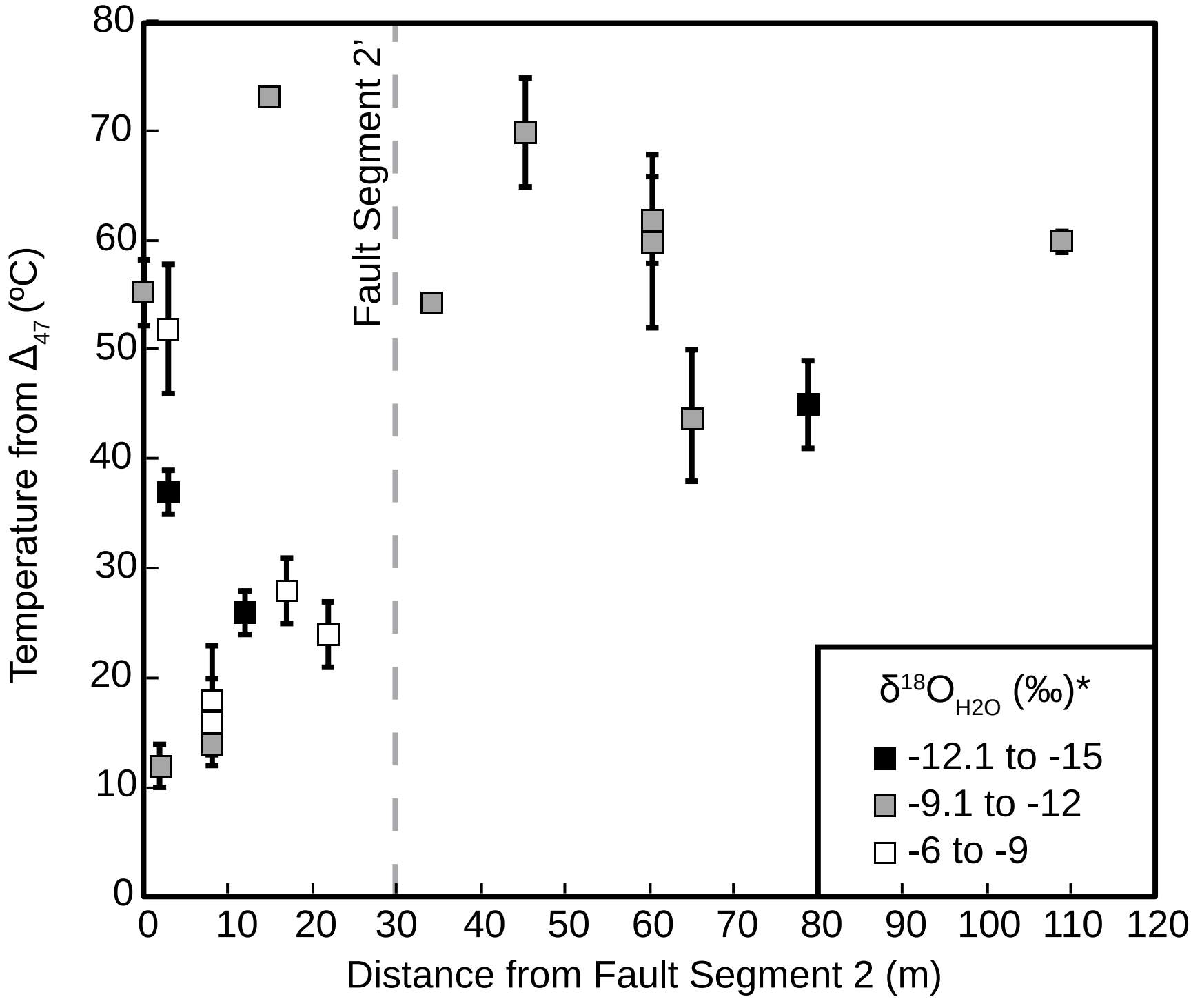
Temperature from Δ_{47} (ºC)
Distance from Fault Segment 2 (m)
Fault Segment 2'
$\delta^{18}O_{H2O}$ (‰)*
-12.1 to -15
-9.1 to -12
-6 to -9
0
10
20
30
40
50
60
70
80
90
100
110
120

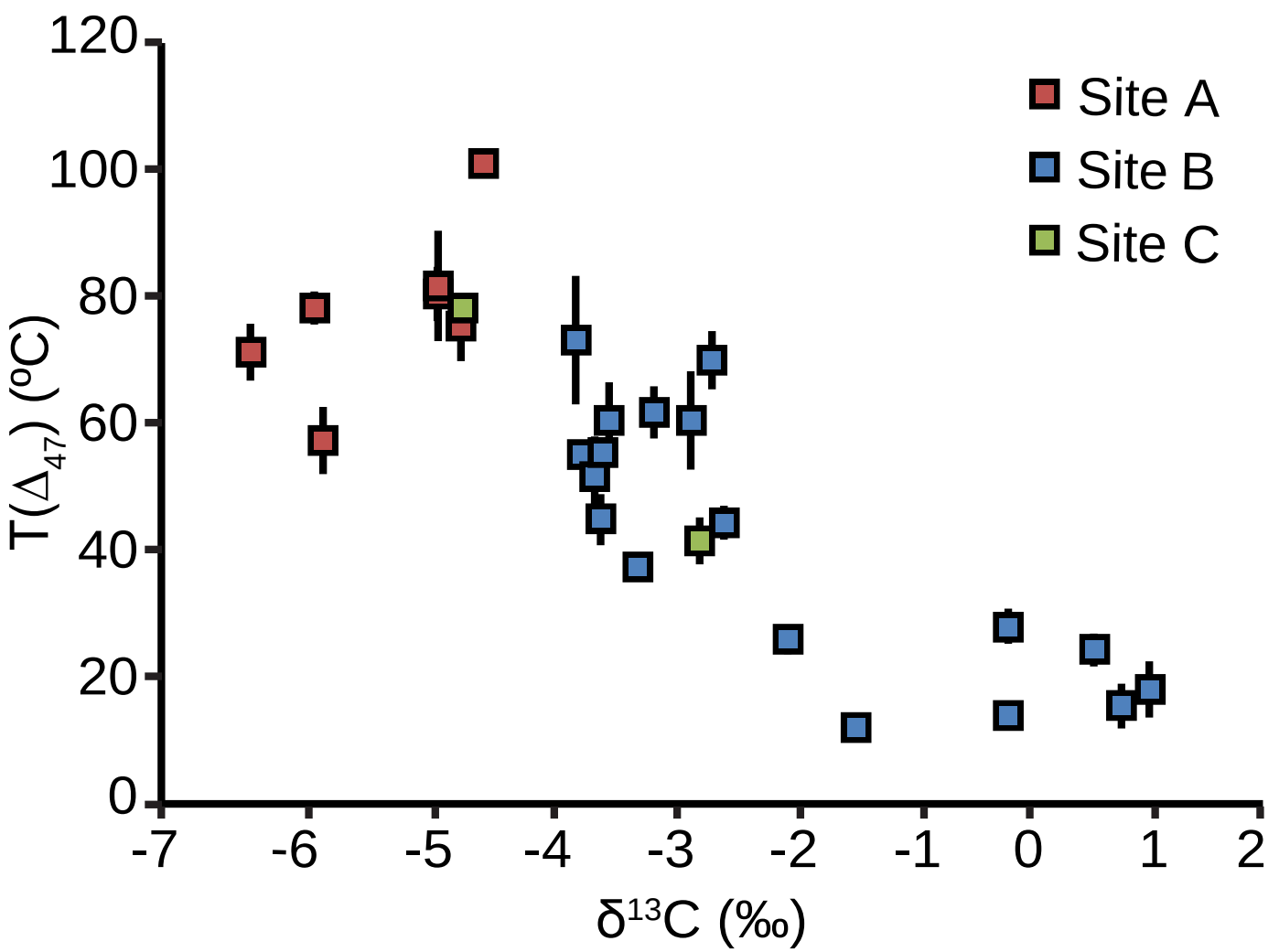
120
100
80
60
40
20
0
T(Δ47) (ºC)
-7
-6
-5
-4
-3
-2
-1
0
1
2
δ13C (‰)
Site A
Site B
Site C

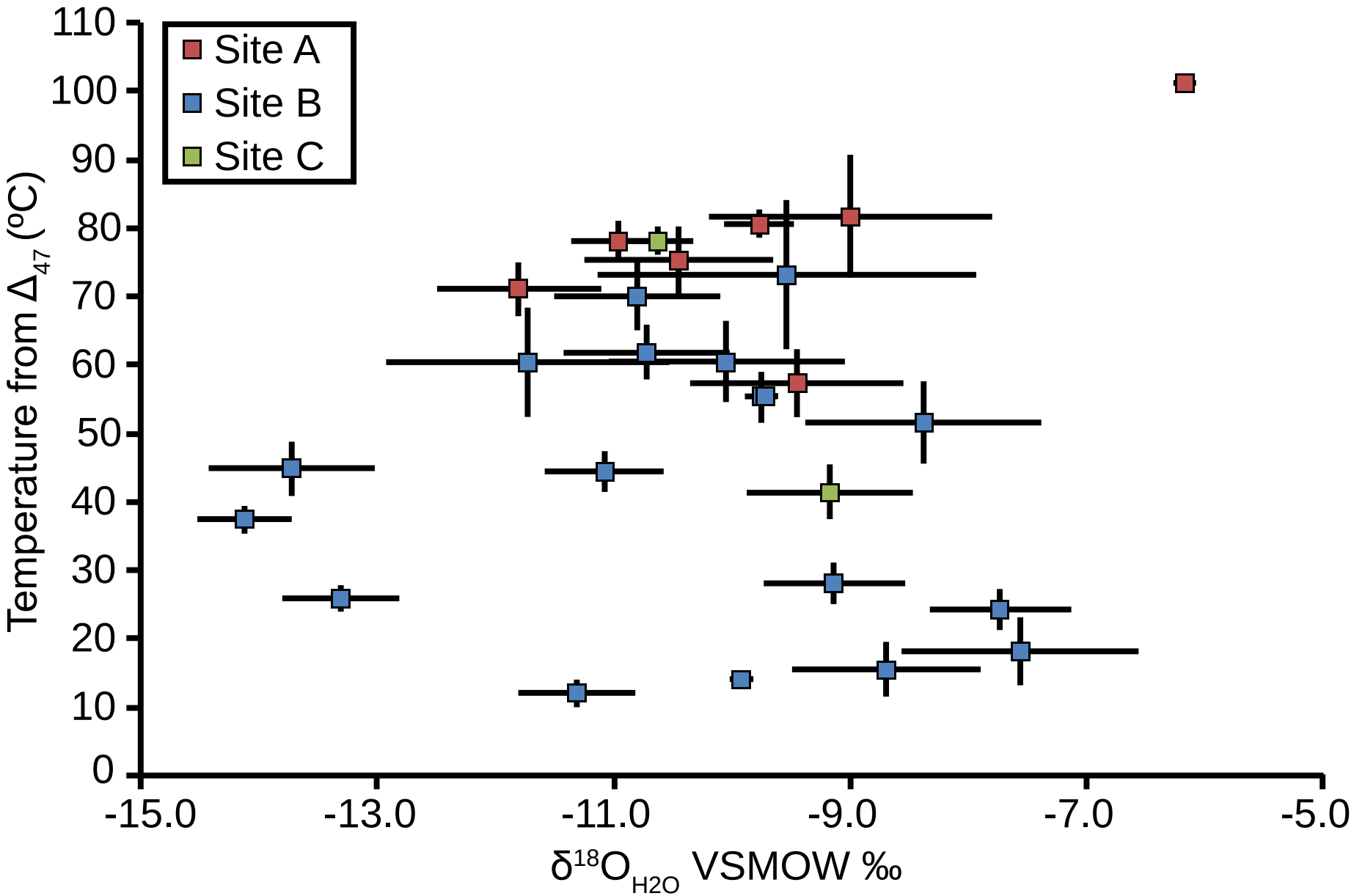
Site A
Site B
Site C
110
100
90
80
70
60
50
40
30
20
10
0
Temperature from Δ47 (ºC)
-15.0
-13.0
-11.0
-9.0
-7.0
-5.0
δ18OH2O VSMOW ‰

Analysis Date	Sample	Distance from Fault Segment 2 (m)	Δ_{47} (‰) ±1 SE	T(Δ_{47}) Guo (ºC) ±1 SE	T(Δ_{47}) Ghosh (ºC) ±1 SE	δ^{18}Ogas† (‰)	$\delta^{18}O_{carb}$ (‰)* ±1 SE	$\delta^{18}O_{H2O}$ (‰)# ±1 SE	δ^{13}C (‰)** ±1 SE
Site A, Navajo Sandstone at Fault Splay 5									
8/22/11	11SB05a	-	0.506 ± 0.004	81 ± 2	62 ± 1	17.016	-21.5 ± 0.1	-9.8 ± 0.6	-4.75 ± 0.06
8/22/11	11SB05b	-	0.504 ± 0.016	82 ± 9	63 ± 5	17.65	-20.9 ± 0.1	-9.0 ± 0.6	-4.74 ± 0.06
8/22/11	11SB05c	-	0.516 ± 0.010	75 ± 5	59 ± 3	17.093	-21.4 ± 0.1	-10.5 ± 0.6	-4.55 ± 0.06
8/25/11	11SB07a1	-	0.516 ± 0.009	75 ± 5	59 ± 3	16.287	-22.164 ± 0.006	-11.2 ± 0.7	-5.790 ± 0.001
8/23/11	11SB07a2	-	0.506 ± 0.008	81 ± 4	62 ±3	16.038	-22.404 ± 0.006	-10.7 ± 0.6	-5.675 ± 0.002
-	11SB07a	-	0.511 ± 0.005	78 ± 3	61 ± 2	16.2	-22.3 ± 0.1	-11.0 ± 0.4	-5.75 ± 0.06
8/25/11	11SB07c	-	0.554 ± 0.012	57 ± 5	48 ± 3	21.010	-17.6 ± 0.1	-9.5 ± 0.6	-5.67 ± 0.06
8/26/11	11SB07b1	-	0.518 ± 0.006	74 ± 3	59 ± 2	16.365	-22.089 ± 0.003	-11.3 ± 0.5	-6.248 ± 0.001
8/23/11	11SB07b2	-	0.536 ± 0.011	65 ± 5	53 ± 3	16.335	-22.119 ± 0.004	-12.7 ± 0.8	-6.346 ± 0.002
-	11SB07b	-	0.524 ± 0.009	71 ± 4	57 ± 3	16.35	-22.10 ± 0.02	-11.8 ± 0.7	-6.27 ± 0.05
9/10/10	10SB20§	-	0.472 ± 0.009	100 ± 6	74 ± 3	17.833	-20.715 ± 0.006	-6.4 ± 0.7	-4.376 ± 0.001
9/11/10	10SB20§	-	0.469 ± 0.008	102 ± 5	75 ± 3	17.977	-20.577 ± 0.006	-6.0 ± 0.7	-4.335 ± 0.001
-	10SB20§	-	0.471 ± 0.002	101 ± 1	74 ± 1	17.9	-20.6 ± 0.1	-6.2 ± 0.1	-4.36 ± 0.03
Site B, Moab Member of Curtis Formation at Courthouse Rock									
9/3/10	10SB07	0	0.558 ± 0.010	56 ± 4	47 ± 3	21.1640	-17.5105 ± 0.0004	-9.6 ± 0.7	-3.5636 ± 0.0004
9/10/10	10SB07§	0	0.559 ± 0.008	55 ± 3	47 ± 2	20.987	-17.681 ± 0.004	-9.9 ± 0.6	-3.5641 ± 0.0004
-	10SB07	0	0.559 ± 0.001	55 ± 4	47 ± 2	21.08	-17.53 ± 0.09	-9.8 ± 0.1	-3.5639 ± 0.0003
8/31/10	10SB09	0	0.594 ± 0.012	41 ± 5	37 ± 3	21.562	-17.127 ± 0.001	-11.8 ± 0.8	-2.3726 ± 0.0005
9/2/10	10SB09	0	0.591 ± 0.010	42 ± 4	38 ± 3	21.6530	-17.0397 ± 0.0004	-11.5 ± 0.7	-2.4434 ± 0.0002
9/8/10	10SB09§	0	0.573 ± 0.007	49 ± 3	43 ± 2	21.618	-17.074 ± 0.001	-10.3 ± 0.5	-2.3764 ± 0.0003
-	10SB09	0	0.586 ± 0.007	44 ± 3	39 ± 2	21.61	-17.07 ± 0.05	-11.2 ± 0.5	-2.40 ± 0.04
8/22/11	11SB09	2	0.676 ± 0.007	12 ± 2	18 ± 1	27.960	-10.9 ± 0.1	-11.3 ± 0.6	-1.33 ± 0.06
8/21/11	11SB16	3	0.609 ± 0.009	35 ± 3	34 ± 2	19.820	-18.766 ± 0.003	-14.5 ± 0.6	-3.080 ± 0.001
8/26/11	11SB16	3	0.597 ± 0.008	39 ± 3	37 ± 2	19.659	-18.921 ± 0.005	-13.8 ± 0.6	-3.119 ± 0.001
-	11SB16	3	0.603 ± 0.006	37 ± 2	35 ± 1	19.74	-18.82 ± 0.08	-14.1 ± 0.4	-3.10 ± 0.02
9/10/10	10SB08§	3	0.582 ± 0.010	45 ± 4	41 ± 3	23.097	-15.651 ± 0.002	-9.5 ± 0.7	-3.4721 ± 0.0003
9/6/10	10SB08§	3	0.553 ± 0.009	57.69 ± 3.86	48 ± 2	23.156	-15.594 ± 0.001	-7.3 ± 0.6	-3.4408 ± 0.0002
-	10SB08§	3	0.567 ± 0.015	52 ± 6	44 ± 4	23.13	-15.62 ± 0.04	-8.4 ± 1.0	-3.45 ± 0.02
8/24/11	11SB18b1	8.1	0.646 ± 0.007	22 ± 2	25 ± 2	30.449	-8.539 ± 0.003	-6.8 ± 0.5	0.976 ± 0.002
8/27/11	11SB18b2	8.1	0.673 ± 0.010	13 ± 3	19 ± 2	30.573	-8.419 ± 0.007	-8.6 ± 0.7	1.103 ± 0.001
-	11SB18b	8.1	0.657 ± 0.014	18 ± 5	23 ± 3	30.51	-8.50 ± 0.06	-7.6 ± 1.0	1.07 ± 0.06
8/24/11	11SB18a1	8.1	0.668 ± 0.010	15 ± 3	20 ± 2	29.061	-9.874 ± 0.006	-9.7 ± 0.7	-0.025 ± 0.001
8/26/11	11SB18a2	8.1	0.671 ± 0.012	14 ± 4	20 ± 3	28.798	-10.127 ± 0.006	-10.2 ± 0.8	-0.164 ± 0.002
-	11SB18a	8.1	0.669 ± 0.002	14 ± 1	20 ± 0	28.9	-10.0 ± 0.1	-9.9 ± 0.1	-0.08 ± 0.07
8/24/11	11SB18c	8.1	0.665 ± 0.011	16 ± 4	21 ± 2	29.833	-9.1 ± 0.1	-8.7 ± 0.6	0.85 ± 0.06
8/27/11	11SB19	12.1	0.642 ± 0.014	23 ± 5	26 ± 3	22.868	-15.832 ± 0.006	-13.9 ± 1.0	-1.834 ± 0.001
8/21/11	11SB19	12.1	0.629 ± 0.009	28 ± 3	29 ± 2	22.876	-15.825 ± 0.002	-13.0 ± 0.6	-1.930 ± 0.001
-	11SB19	12.1	0.634 ± 0.007	26 ± 2	28 ± 1	22.875	-15.827 ± 0.004	-13.3 ± 0.5	-1.88 ± 0.05
9/5/10	10SB11§	15	0.499 ± 0.009	84 ± 5	65 ± 3	18.229	-20.334 ± 0.005	-8.1 ± 0.7	-3.6231 ± 0.0005
9/8/10	10SB11§	15	0.542 ± 0.011	63 ± 5	52 ± 3	18.4274	-20.1434 ± 0.0006	-11.1 ± 0.8	-3.6105 ± 0.0003
-	10SB11§	15	0.520 ± 0.021	73 ± 11	58 ± 7	18.3	-20.2 ± 0.1	-10 ± 2	-3.61 ± 0.01
8/27/11	11SB20	17	0.628 ± 0.008	28 ± 3	29 ± 2	26.757	-12.1 ± 0.1	-9.1 ± 0.6	-0.08 ± 0.06
8/28/11	11SB22	21.8	0.633 ± 0.005	26 ± 2	28 ± 1	28.940	-9.990 ± 0.005	-7.4 ± 0.3	0.492 ± 0.002
8/28/11	11SB22	21.8	0.648 ± 0.003	21 ± 3	25 ± 2	29.025	-9.909 ± 0.003	-8.3 ± 0.6	0.653 ± 0.001
-	11SB22	21.8	0.639 ± 0.008	24 ± 3	27 ± 2	28.24	-9.94 ± 0.04	-7.7 ± 0.6	0.62 ± 0.08
8/25/11	11SB24	45.3	0.518 ± 0.011	74 ± 6	59 ± 3	17.773	-20.735 ± 0.003	-9.9 ± 0.8	-2.624 ± 0.001
8/26/11	11SB24	45.3	0.537 ± 0.013	65 ± 6	53 ± 4	16.922	-21.554 ± 0.009	-12.2 ± 1.0	-2.387 ± 0.001
-	11SB24	45.3	0.527 ± 0.010	70 ± 5	56 ± 3	17.3	-20.9 ± 0.4	-10.8 ± 0.7	-2.5 ± 0.1
8/24/11	11SB25a	60.3	0.547 ± 0.017	60 ± 8	50 ± 5	18.140	-20.4 ± 0.1	-12 ± 0.6	-2.68 ± 0.06
8/25/11	11SB25b	60.3	0.544 ± 0.009	62 ± 4	51 ± 3	18.953	-19.6 ± 0.1	-10.7 ± 0.6	-2.98 ± 0.06
8/27/11	11SB26	78.8	0.592 ± 0.009	41 ± 4	38 ± 2	18.95	-19.60 ± 0.01	-14.2 ± 0.6	-3.408 ± 0.002
8/21/11	11SB26	78.8	0.572 ± 0.012	50 ± 5	43 ± 3	18.714	-19.829 ± 0.003	-13.0 ± 0.9	-3.413 ± 0.001
-	11SB26	78.8	0.583 ± 0.010	45 ± 4	40 ± 3	18.8	-19.8 ± 0.1	-13.7 ± 0.7	-3.411 ± 0.003
9/12/10	10SB13§	109	0.534 ± 0.009	66 ± 4	54 ± 3	19.830	-18.794 ± 0.001	-9.2 ± 0.6	-3.3868 ± 0.0003
9/9/10	10SB13§	109	0.550 ± 0.010	59 ± 5	49 ± 3	19.9340	-18.6941 ± 0.0004	-10.2 ± 0.7	-3.2876 ± 0.0003
-	10SB13	109	0.547 ± 0.013	60 ± 6	50 ± 4	19.88	-18.73 ± 0.07	-10.1 ± 1.0	-3.34 ± 0.07
9/3/10	10SB15	34	0.556 ± 0.009	56 ± 4	47 ± 2	21.353	-17.329 ± 0.005	-9.3 ± 0.6	-3.3173 ± 0.0004
9/10/10	10SB15§	34	0.560 ± 0.008	55 ± 3	46 ± 2	21.052	-17.618 ± 0.001	-9.9 ± 0.6	-3.4439 ± 0.0003
-	10SB15	34	0.558 ± 0.002	55 ± 1	47 ± 0	21.2	-17.6 ± 0.2	-9.7 ± 0.1	-3.39 ± 0.09
Site C, Curtis Formation at Mill Canyon									
9/1/10	10SB25	-	0.517 ± 0.010	75 ± 5	59 ± 3	16.997	-21.52 ± 0.001	-10.7 ± 0.8	-4.6084 ± 0.0004
9/11/10	10SB25§	-	0.504 ± 0.010	82 ± 5	63 ± 3	16.2690	-22.2200 ± 0.0004	-10.4 ± 0.8	-4.4476 ± 0.0003
9/8/10	10SB25§	-	0.511 ± 0.001	78 ± 4	61 ± 2	15.982	-22.496 ± 0.001	-11.2 ± 0.5	-4.4890 ± 0.0003
-	10SB25	-	0.511 ± 0.004	78 ± 2	61 ± 1	16.4	-22.0 ± 0.5	-10.7 ± 0.3	-4.53 ± 0.08
9/11/10	10SB26§	-	0.602 ± 0.011	38 ± 4	35 ± 3	24.204	-14.586 ± 0.001	-9.83 ± 0.8	-2.5020 ± 0.0003
9/4/10	10SB26§	-	0.583 ± 0.009	45 ± 4	40 ± 2	23.847	-14.929 ± 0.006	-8.8 ± 0.6	-2.922 ± 0.001
-	10SB26	-	0.592 ± 0.009	41 ± 4	38 ± 2	24.0	-14.6 ± 0.2	-9.2 ± 0.7	-2.6 ± 0.3

Note: Grey rows represent weighted means of replicates of the same sample. Samples starting with '10' include vein and halo calcite; samples starting with '11' contain only vein calcite. Sample names with a, b, and c indicate samples representing different stages of growth in the same crystal, with "a" predating "b" and "b" predating "c".

†Samples are referenced to VSMOW

*Samples are referenced to VPDB; ±0.1‰ external error (1 SE) etimated for samples with one analysis based on average error for externally replicated samples

#Values referenced to VSMOW. Uncertainty based on propogating error in T(Δ47) and δ18Ocarb through the calcite-water O-isotope fractionation equation of Kim and O'Neil (1997); ±0.6‰ external error (1 SE) estimated for samples with one anaysis based on average error for replicated samples

**Values referenced to VPDB; ±0.06‰ external error (1 SE) estimated for samples with one analysis based on average error for exernally replicated samples

§ Indicates sample was cleaned in H_2O_2 solution. Not all samples processed in 2010 were cleaned. All samples processed in 2011 were cleaned.

Table 2. ICP-OES Results

Sample	Ba/Ca	Sr/Ca	Ba (ppb)	Sr (ppb)	Ca (ppm)
Site A, Navajo Sandstone at Fault Splay 5					
11SB07	-0.007	1.682	-0.140	33.701	20.036
11SB05	-0.029	2.466	-0.908	77.439	31.408
Site B, Moab Member of Curtis Formation at Courthouse Rock					
11SB09	0.120	0.639	2.051	10.906	17.062
11SB16	-0.053	0.959	-0.481	8.768	9.143
11SB19	-0.064	0.785	-0.393	4.816	6.137
11SB24	0.003	1.316	0.082	33.034	25.102
11SB25	0.084	0.848	2.030	20.473	24.144
11SB26	0.129	0.913	2.295	16.293	17.852